Crystal Structures of an O-Like Blue Form and an Anion-Free Yellow Form of pharaonis Halorhodopsin

ARTICLE *in* JOURNAL OF MOLECULAR BIOLOGY · AUGUST 2011

Impact Factor: 4.33 · DOI: 10.1016/j.jmb.2011.08.021 · Source: PubMed

5 AUTHORS, INCLUDING:

Kunio Ihara
Nagoya University
59 PUBLICATIONS **1,027** CITATIONS

SEE PROFILE

Tsutomu Kouyama
Nagoya University
69 PUBLICATIONS **2,045** CITATIONS

SEE PROFILE

PROTEINS
STRUCTURE ■ FUNCTION ■ BIOINFORMATICS

Crystal structure of the O intermediate of the Leu93→Ala mutant of bacteriorhodopsin

Jin Zhang,[1] Yoshikazu Yamazaki,[1] Masanori Hikake,[1] Midori Murakami,[1] Kunio Ihara,[2] and Tsutomu Kouyama[1,3]*

[1] Department of Physics, Graduate School of Science, Nagoya University, Nagoya 464-8602, Japan

[2] Center for Gene Research, Nagoya University, Nagoya 464-8602, Japan

[3] RIKEN Harima Institute/SPring-8, Hyogo 679-5148, Japan

ABSTRACT

The lifetime of the O intermediate of bacteriorhodopsin (BR) is extended by a factor of ~250 in the Leu93-to-Ala mutant (BR_L93A). To clarify the structural changes occurring in the last stage of the proton pumping cycle of BR, we crystallized BR_L93A into a hexagonal *P622* crystal. Diffraction data from the unphotolyzed state showed that the deletion of three carbon atoms from Leu93 is compensated by the insertion of four water molecules in the cytoplasmic vicinity of retinal. This insertion of water is suggested to be responsible for the blue-shifted λ_{max} (540 nm) of the mutant. A long-lived substate of O with a red-shifted λ_{max} (~565 nm) was trapped when the crystal of BR_L93A was flash-cooled after illumination with green light. This substate (O_{slow}) bears considerable similarity to the M intermediate of native BR; that is, it commonly shows deformation of helix C and the FG loop, downward orientation of the side chain of Arg82, and disruption of the Glu194/Glu204 pair. In O_{slow}, however, the main chain of Lys216 is less distorted and retinal takes on the 13-*cis*/15-*syn* configuration. Another significant difference is seen in the pH dependence of the structure of the proton release group, the pK_a value of which is suggested to be much lower in O_{slow} than in M.

Proteins 2012; 80:2384–2396.

Key words: retinal protein; proton pump; O intermediate; retinal isomerization; X-ray crystallography.

INTRODUCTION

Bacteriorhodopsin (BR), a transmembrane retinylidene protein discovered in the cell membrane of the extremely halophilic archaeon *Halobacterium salinarum*, is a light-driven proton pump that transports protons against an electrochemical gradient from the cytoplasmic to the extracellular side.[1–4] Each cycle of proton transport is initiated by photoisomerization of the covalently attached all-*trans* retinal chromophore to the 13-*cis*/15-*anti* configuration. It has been widely accepted that five spectroscopically distinct intermediates (K, L, M, N, and O) occur in the *trans* photocycle.[5–7] The structures of the K, L, M intermediates of native BR have been characterized using X-ray crystallography in recent years.[8–20] In these studies, the *P622* crystal prepared by the membrane fusion method and the $P6_3$ crystal prepared by the lipidic cubic phase method have been utilized. Since there are some discrepancies between the reported structural models of these reaction intermediates, it is not necessarily the case that the same conformational change is induced in the different crystal forms. Diffraction data from the *P622* crystal have shown that the following structural changes takes place:[10,12,19,20] (1) in the L intermediate, the Schiff base NH bond interacts with a water molecule that is relocated to an open space generated by rotation of the side chain of Leu93; (2) in the L-to-M transition, this water moves away from the Schiff base, causing a significant reduction of the pK_a value of the Schiff base; (3) complete proton transfer from the retinal Schiff base to Asp85 occurs when the proton release pathway undergoes a large structural change in the M intermediate, including disruption of the paired structure of Glu194

Additional Supporting Information may be found in the online version of this article.

Abbreviations: BR, bacteriorhodopsin; BR_L93A, L93A mutant of bacteriorhodopsin; O_{slow}, a long-live substate of the O intermediate in BR_L93A.

Grant sponsor: Ministry of Education, Science, and Culture of Japan.
*Correspondence to: Tsutomu Kouyama, Department of Physics, Graduate School of Science, Nagoya University, Chikusa-Ku, Nagoya 464-8602, Japan.
E-mail: kouyama@bio.phys.nagoya-u.ac.jp
Received 21 February 2012; Revised 5 May 2012; Accepted 14 May 2012
Published online 29 May 2012 in Wiley Online Library (wileyonlinelibrary.com).
DOI: 10.1002/prot.24124

and Glu204. With respect to the N intermediate, its structure was determined by analyzing a light-induced change in the electron density map of the purple membrane of F219L mutant of BR.[21] It was suggested that the cytoplasmic half of helix F deforms largely in the N intermediate. This large structural change was not detected in the $P6_3$ crystal, probably because of inherent constraint by the three-dimensional crystal lattice.[22]

Although the early half of the photocycle of BR has been well analyzed, the mechanism of re-isomerization of retinal taking place in the last half of the proton pumping cycle has been poorly understood. Recently, the crystal structures of the unphotolyzed state of the D85S mutant[23] and the acid blue form of native BR[24] were reported to mimic the O intermediate. Unfortunately, these putative O-like structures are not strongly correlated. One of the most prominent differences involves an important water molecule Wat602 (Wat402 in the D85S mutant) that connects the Schiff base and Asp85 in the unphotolyzed state of native BR. In the non-illuminated D85S mutant, this water still exists in the vicinity of the Schiff base, while the Schiff base interacts directly with Asp85 in the acid blue form of native BR. Up to date, little structural information has been provided for the O intermediate generated under light illumination. Difficulties associated with this structural analysis stem from the similar decay rates for M, O, and N.

The Leu93→Ala mutant (BR_L93A) is an excellent candidate for structural investigation of the O intermediate, because the lifetime of O in BR_L93A is extended by a factor of ~250 compared with native BR.[25] A previous structural analysis of the purple membrane of BR_L93A by electron microscopy suggested that significant structural changes occurred in the vicinity of helices C, B, and G upon formation of the O intermediate.[26,27] But no information was provided about the retinal configuration in the O intermediate, which has been a matter of controversy. It has previously been reported that the retinal re-isomerization takes place in the N-to-O transition for native BR.[5] Contrary to this general notion, Subramaniam *et al.* observed that retinal took on the 13-*cis* configuration in the O intermediate of BR_L93A.[25] In their preferred reaction scheme, the presence of the long-lived O intermediate was attributed to the inhibition of the thermal isomerization of retinal. Conversely, Toth-Boconadi *et al.* reported that two substates of O occurred in the photocycle of BR_L93A and that the retinal took on all-*trans* configuration in the long-lived substate of O.[28] To clarify retinal re-isomerization or water relocation in the last half of the photocycle, therefore, it is important to prepare such a three-dimension crystal that allows a high-resolution structural analysis of the O intermediate.

In this study, BR_L93A was crystallized into hexagonal *P622* crystals, and diffraction data from the unphotolyzed state and from the long-lived substate of O (O_{slow}) were collected at 2.3 Å resolution. Structural comparison of the *trans* isomers of BR_L93A and native BR showed that while the whole protein structure is little affected by the mutation, the cavity created by the Leu93→Ala replacement is occupied by four additional water molecules. Meanwhile, the structural data of O_{slow} showed that this reaction state bears considerable similarity to the M intermediate of native BR at pH 7.0 (M_{native}). For example, distortion of the extracellular half of helix C, destruction of the paired structure of Glu194 and Glu204, and flip-flop motion of the side chain of Arg82 toward the extracellular side are also seen in these states. However, there is a noticeable difference in that the main-chain structure of Lys216 is less distorted in O_{slow} than in M_{native}. This difference is attributed to a difference in the configuration of retinal; that is, the retinal in O_{slow} takes on the 13-*cis*/15-*syn* configuration, while the retinal in M_{native} takes on the 13-*cis*/15-*anti* configuration. This implies that the retinal isomerization from the all-*trans* to the 13-*cis*/15-*syn* configuration takes place during the elongation of the lifetime of O in BR_L93A. The structural data obtained in this study provide an insight into the mechanism underlying the re-isomerization of retinal in the proton pumping cycle of BR.

MATERIALS AND METHODS

Plasmid construction and site-directed mutation

A bacterioopin (*bop*) gene fragment containing 5′ and 3′ flanking regions (each 400 bp) was cloned into the *Escherichia coli* plasmid vector pUC18. A point mutation at Leu93 to Ala was introduced into the *bop* gene by the inverse PCR method using the following two primers: 5′-CAA**CGC**CAGCGGCGTGGTGAACAGCC-A-3′, and 5′-TTAGACCTCGCGTTGCT-CGTTGACGCG-3′. Following confirmation of the site of mutation in the *bop* gene sequence, the *bop* gene fragment was cloned into the homologous recombination vector pKI72, consisting of the mevinoline-resistance marker gene, the ampicillin-resistance marker gene, and the replication origin for *E. coli*. The host strain was MPK409, which was a generous gift from Dr. Mark P. Krebs. Transformation was performed according to Cline *et al.*[29] with slight modifications. Positive selection with simvastatine and negative selection with 5-FOA in the presence of uracil led to complete substitution of the *ura3* gene with the L93A-*bop* gene.[30]

Protein purification and crystallization

Purple membrane was isolated from *Halobacterium salinarum* strain MPK409 (L93A-bop) and purified accord-

ing to standard procedures.[31] Crystals were grown by the membrane fusion method[32] with slight modifications.

Measurement of absorption spectra and kinetics

The absorption spectra of a crystal of BR_L93A were measured using a microspectrophotometer, in which monochromatic light from a double monochromator (Shimadzu UV350A) was passed through a pin-hole with a diameter of 0.2 mm and focused on a small area of the crystal.[33]

The absorption spectra of a purple membrane suspension under light illumination were measured using a cross-illumination spectrophotometer, in which the actinic light and the measuring light were alternately chopped at a frequency of 200 Hz.[34] Transient transmission data were acquired using a computer-controlled experimental setup with a digital oscilloscope, and a frequency-doubled Nd-YAG laser (Quantel Ultra; 3 ns, 532 nm).[35] The kinetic model of Chizhov *et al.*[36] was used for data analysis. Using the singular value decomposition method,[37] the absorption kinetics measured at various wavelengths were decomposed into three major singular value vectors, from which the optimal number of exponential components and individual decay constants were determined.

Data collection and scaling

Diffraction data were collected at SPring-8 beamlines BL38B1 and BL26B2, where a crystal kept at 100K was exposed to a monochromatic X-ray beam at a wavelength of 1.0 Å with an X-ray flux rate of $\sim 2 \times 10^{12}$ photons/mm^2/s. Diffraction data were collected using a CCD detector (ADSC 315), with an oscillation range of 1° and an X-ray flux of $\sim 1 \times 10^{13}$ photons/mm^2 per image. Indexing and integration of diffraction spots were carried out using Mosflm 6.1.[38] The scaling of data was accomplished using SCALA in the CCP4 program suite.[39]

Model building of the *trans* isomer and O_{slow} of BR_L93A

Structural refinement of the *trans* isomer of BR_L93A was carried out using CNS version 1.2,[40] beginning with 1IW6 as an initial model. Initial refinement consisted of rounds of simulated annealing and B-factor refinement. The difference maps were displayed using the Xtal-view/Xfit program[41] for model corrections.

The structural model of O_{slow} of BR_L93A was constructed using the diffraction data (F_{green}) from a crystal that was flash-cooled 0.5 s after green-light illuminated was terminated and those (F_{red}) from a crystal that was flash-cooled in red light (650 nm). On the approximation that O_{slow} took on a homogenous conformation when trapped in the crystal, its structure was refined so as to explain the diffraction amplitude, $|F_{obs\text{-}O\text{-}slow}|$, that was evaluated using the equation: $|F_{obs\text{-}O\text{-}slow}| = |F_{red}| + (|F_{green}| - |F_{red}|)/\alpha$, where α is the occupancy of O_{slow} in the crystal that was flash-cooled after green-light illumination. The parameter α was varied until a structural model was obtained in which the density map around Arg82 was clearest. To check the approximation used in the above model building, we performed another procedure of refinement in which the observed amplitude $|F_{green}|$ was compared with a weighted average of the calculated amplitudes, $|F_{calc\_O\_slow}|$ and $|F_{calc\_Trans}|$, from the two conformers (O_{slow} and the *trans* isomer); i.e., $|F_{calc}| = \alpha \cdot |F_{calc\_O\_slow}| + (1 - \alpha) \cdot |F_{calc\_Trans}|$; here, the structure of O_{slow} was refined by the simulated annealing method, while the structure of the other conformer was assumed to be identical to the *trans* isomer in a crystal that was flash cooled in red light. In this refinement, the optimal value of α was estimated by investigating the crystallographic *R* values evaluated at various α values (see Supporting Information Fig. S4).

RESULTS

Crystal structure of the *trans* isomer of BR_L93A

When the membrane fusion method[32] was applied, BR_L93A crystallized into a hexagonal crystal belonging to space group *P622*, which diffracted X-rays up to a resolution of 2.3 Å (Supporting Information Table S1). The lattice constants of this crystal were similar to those observed for the *P622* crystal of native BR, allowing us to construct a difference map between BR_L93A and native BR [Fig. 1(A)]. This shows that the protein structure was barely affected by the deletion of three carbon atoms in Leu93. However, in BR_L93A, four additional water molecules (Wat701 to 704) were observed in a cavity created around Ala93. Together with the water molecule (Wat601) that exists in native BR, these water molecules form a hydrogen-bonding network between the indole nitrogen of Trp182 and the main-chain carbonyl of Lys216. The formation of the water cluster in this region is accompanied by a small movement of the indole ring of Trp182 toward helix E. A similar movement of Trp182 has been reported to take place upon the formation of the L intermediate of native BR, in which the side chain of Leu93 rotates to create a large cavity accommodating two water molecules in the cytoplasmic vicinity of retinal.[12] In this respect, the structure of BR_L93A is similar to that of the L intermediate of native BR. The present result is in line with the previous FT-IR data showing that the L93M and W182F mutations induce changes in the hydrogen bonding of water molecules in the cytoplasmic vicinity of retinal.[42]

The structural model of the L93A mutant shown in Figure 1(B) was constructed using the diffraction data

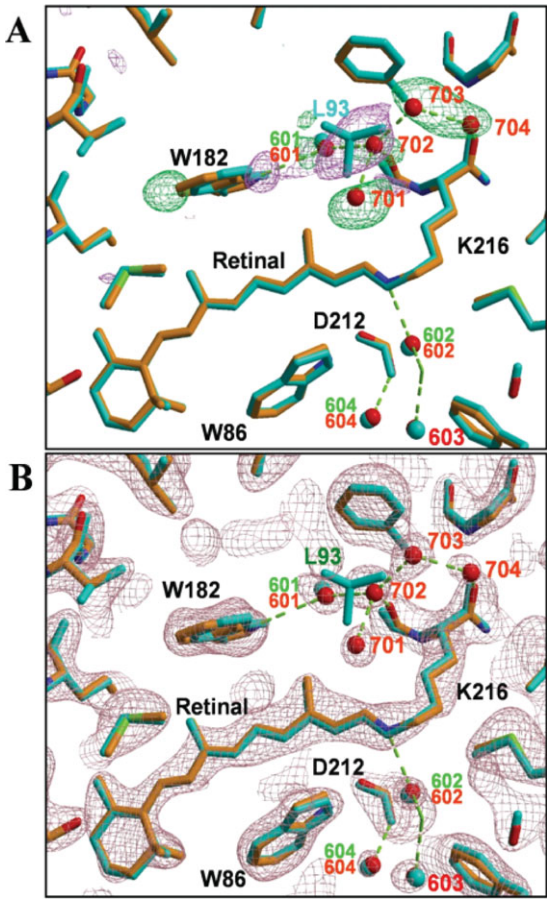

Figure 1

Insertion of four water molecules into a cavity created by the Leu93→Ala replacement. (**A**) $|F_{T\text{-}L93A}| - |F_{T\text{-}native}|$ difference map between the *trans* isomer of BR_L93A and that of native BR, contoured at 4 σ (positive densities in cyan, negative in purple) and overlaid on their structural models. For derivation of this difference map, the diffraction data ($|F_{T\text{-}L93A}|$) were collected from a *P622* crystal of BR_L93A that was soaked in 3*M* ammonium sulfate at pH 7.0 and then flash-cooled under illumination with red light at 650 nm, and compared with those ($|F_{T\text{-}native}|$) from a light-adapted crystal of native BR. (**B**) $2F_o\text{-}F_c$ map of the *trans* isomer of BR_L93A, contoured at 1.8 σ. Carbon, nitrogen, and oxygen atoms in the mutant are drawn in gold, blue, and red, respectively, while all the atoms in native BR are shown in cyan.

from a crystal that was flash-cooled under illumination with red light at 650 nm (and kept in red light during data collection). Based on the density maps around the internal water molecules, the protein conformation in this crystal state appeared to be more homogenous than that observed in crystals that were frozen in dim light. It seems possible that red light is effective at removing an O-like protein conformer that might accumulate in dim light. The diffraction data from a crystal that was frozen in red light suggest that the retinal takes on the all-*trans* configuration, which is almost identical to that found in the light-adapted state of native BR. In the following discussion, this state will be referred as the *trans* isomer.

Flash-induced absorption changes in a membrane suspension of BR_L93A

Figure 2(A) shows the absorption changes observed when a membrane suspension of BR_L93A at pH 7.0 was excited with light pulses at 532 nm. In the investigated time region, the absorption kinetics measured at various wavelengths were fitted with five exponential compo-

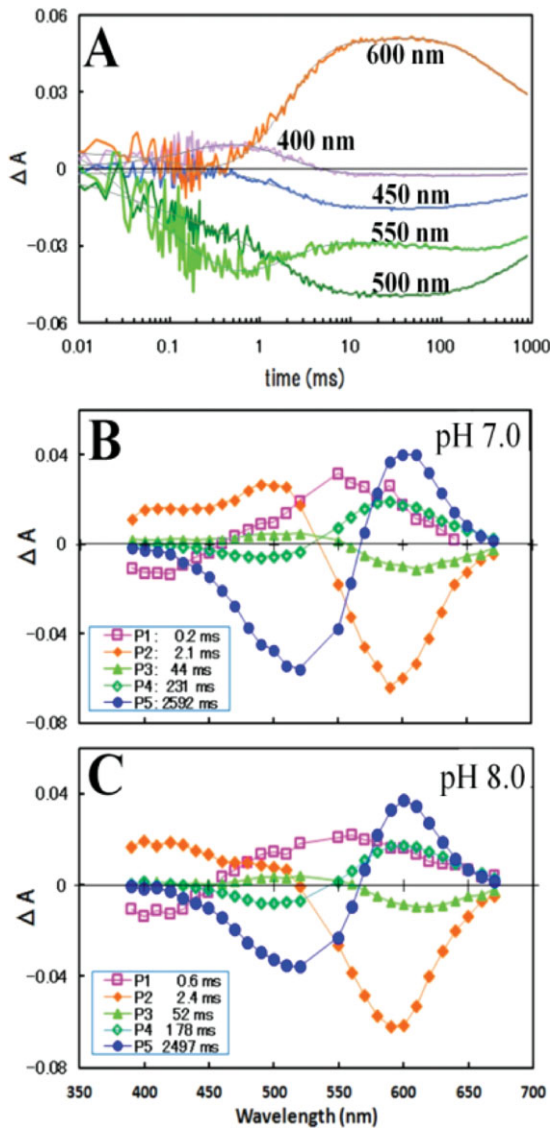

Figure 2

(**A**) Flash-induced absorption changes in a membrane suspension of BR_L93A at pH 7.0 (0.1*M* Hepes buffer, 200 m*M* NaCl, 24°C) were recorded at various wavelengths. The observed absorption changes (zigzag lines) were fitted with five exponential components; P_1: τ = 0.20 ms, P_2: τ = 2.1 ms, P_3: τ = 44 ms, and P_4: τ = 231 ms, P_5: τ = 2.59 s. (**B**) The amplitude of each exponential component is plotted against the wavelength of the measuring light. (**C**) The data observed for a membrane suspension at pH 8.0 (0.1*M* Hepes buffer, 200 m*M* NaCl, 24°C). [Color figure can be viewed in the online issue, which is available at wileyonlinelibrary.com.]

nents. In Figure 2(B), the amplitudes of the individual components are plotted against the wavelength of the measuring light. The P_1 component, which is characterized by a negative value at 410 nm, is attributable to the L-to-M transition. The P_2 component, which has a negative value at 610 nm, is attributable to the rising phase of a reaction state with a red-shifted absorption spectrum. The difference spectrum associated with the P_2 component, which has a twin peak at 410 nm and 500 nm, suggests that an equilibrium state of L and M is established at a much faster rate than the decay rate of M. In fact, it was observed that the transient concentration of M increased monotonically when the pH of the medium was increased from pH 7.0 to pH 8.0 [Fig. 2(C)]. This pH dependence suggests that the L intermediate is in dynamic equilibrium with the M intermediate,[43] and that the pK_a value of the Schiff base in the M intermediate of BR_L93A is considerably higher (pK_a $\sim$ 8) than that reported for the M intermediate of native BR. It seems possible that the pK_a value of the Schiff base or Asp85 is controlled by the protonation state of the proton release group, as suggested by Balashov *et al.*[43]

The difference spectrum associated with the P_5 component has a positive peak at 600 nm and a negative peak at 500 nm. This component was previously attributed to the decay of the O intermediate into the initial state.[25] For correct interpretation of the kinetics data, however, the P_3 and P_4 components should be taken into account. To explain these components, we need to postulate that three states with red-shifted absorption spectra (as compared with L) occur after the decay of M. The following schemes may be considered: (1) sequential occurrence of three states (N$\rightarrow$ O_1 $\rightarrow$ O_2 $\rightarrow$ *trans*-BR), (2) a side reaction (N$\rightarrow$ O_1 ($\leftrightarrow$ O_2) $\rightarrow$ *trans*-BR), (3) a branching reaction (N$\rightarrow$ O_1 $\rightarrow$ O_2 $\rightarrow$ 13-*cis*-BR$\rightarrow$ *trans*-BR) [Fig. 3(A)]. At present, however, it is not clear which reaction scheme is correct. [The reaction scheme of the *trans* isomer might be simplified if the P_4 component reflects the photochemical reaction of the 13-*cis* isomer, whose content in the light-adapted state is not negligible (Supporting Information Table S2).] The aims of the current study were thus: (i) to identify a suitable procedure for trapping the long-lived substate of O; and (ii) to determine its spectroscopic and structural properties. Hereafter this substate will be called O_{slow}.

For spectral characterization of the O intermediate, the absorption spectrum of a purple membrane suspension of BR_L93A was recorded under illumination with yellow light [Fig. 3(B)]. By subtracting the contribution of the unphotolyzed state from this absorption spectrum, one can calculate the absorption spectrum of O_{slow}., which is expected to accumulate under continuous light illumination. Meanwhile, retinal extraction experiments showed that the content of the 13-*cis* isomer increased to 64% under a similar illumination condition (Supporting Information Table S2). On the approximation that this increase is attributable solely to the accumulation of O_{slow}, the absorption spectrum of O_{slow} [the broken blue line in Fig. 3(B)] was calculated. It is suggested that O_{slow} has an absorption peak at $\sim$565 nm. Interestingly, its absorption coefficient at λ_{max} is much lower than that of the unphotolyzed state. It should be pointed out that the absorption coefficient of the *trans* isomer of BR_L93A at λ_{max} is nearly identical to that of the light-adapted state of native BR (Supporting Information Fig. S1).

The absorption spectrum of O_1 was calculated by combining the absorption spectrum of O_{slow} and the differ-

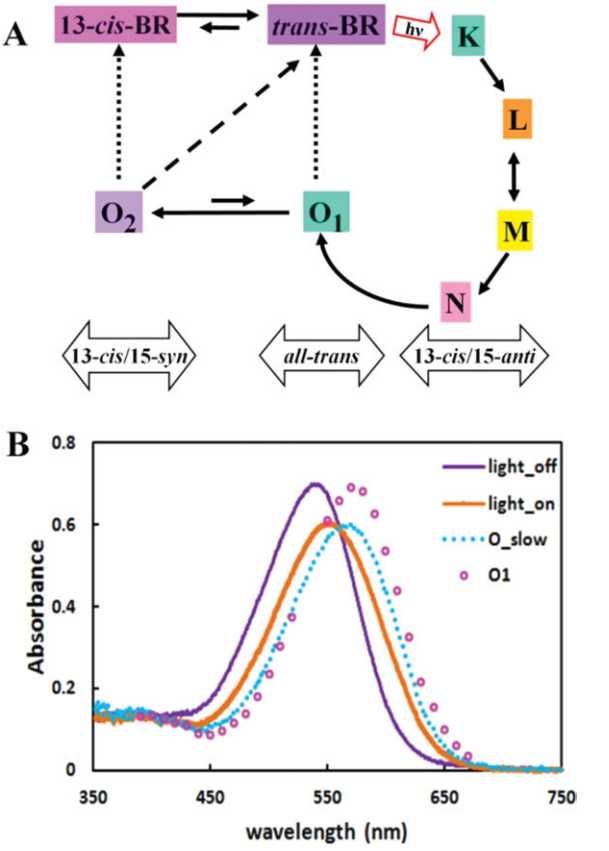

Figure 3

(**A**) Photochemical reactions of the *trans* isomer (*trans*-BR) and the 13-*cis* isomer (13-*cis*-BR) of BR. The reactions that may become significant under some experimental conditions are shown by the broken lines. (**B**) Absorption spectra of a membrane suspension of BR_L93A (0.1*M* Hepes buffer, pH 7.0, 24°C) were measured under continuous illumination with yellow light (>420 nm, ~3 mW/cm^2) (the solid brown line) and in the dark (the solid purple line). The broken blue line represents the absorption spectrum of O_{slow} that is derived when the content of O_{slow} is assumed to be 0% in the dark and 60% under yellow-light illumination. For calculation of the absorption spectrum of O_1 (the open magenta circles), the difference absorption spectrum associated with the P_4 component shown in Figure 2(B) was multiplied by a renormalization factor and then added to the absorption spectrum of O_{slow}. Here, the renormalization factor was determined by comparing the absorption change induced by continuous yellow light and the amplitude of the P_5 component in Figure 2.

ence absorption spectrum associated with the P_4 component (Fig. 2). The absorption spectrum of O_1 shown in Figure 3(B) (the open magenta circles) was derived on the approximation that the P_4 component represents the pure transition from O_1 to O_2 transition. This approximation is fully satisfied when the sequential reaction scheme is adopted. The above approximation is also useful even when another reaction scheme is adopted, provided that the $O_1 \rightarrow O_2$ transition takes place much faster than the recovery of the initial state or the backward reaction ($O_2 \rightarrow O_1$). In this case, the absorption coefficient at λ_{max} of O_1 is similar to that of the unphotolyzed state. This spectral property suggests that retinal in O_1 takes on the all-*trans* configuration; namely, reisomerization from the 13-*trans*/15-*anti* to the 13-*cis*/15-*syn* configuration takes place during the elongated lifetime of O_1 (τ = 231 ms at 24°C).

Effect of the crystal lattice force on the photoreaction kinetics of BR_L93A

It has previously been shown that the decay of the M intermediate of native BR is inhibited when the intermembrane space in the *P622* crystal is reduced at a high concentration of ammonium sulphate.[20] In order to clarify how the crystal lattice force perturbs the photoreaction kinetics of BR_L93A, we measured flash-induced absorption changes of BR_L93A in the *P622* crystal under various solvent conditions (Supporting Information Fig. S2). As observed for native BR, the decay of M in the *P622* crystal of BR_L93A was retarded when the concentration of ammonium sulfate in the postcrystallization solution was increased. This retardation is due to the lattice force effect, by which the motional freedom of the EF loop is suppressed. [In membrane suspensions, the decay rate of M is not significantly affected by the presence of 3*M* ammonium sulfate.] Conversely, the decay rate of O_{slow} was barely affected (or slightly accelerated) when the concentration of ammonium sulfate was increased. This result implies that the structure of the EF loop does not significantly change during the decay of O_{slow}.

At low concentrations of ammonium sulfate, the rising rate of absorbance at 620 nm was noticeably slower than the decay rate of absorbance at 410 nm. This mismatch suggests that a reaction state (i.e., N) whose absorbance is small at these wavelengths (410 nm and 620 nm) occurs between M and O. In the measuring system where the *c* axis of the crystal was parallel to the optical path of the measuring beam, the P_3 component had negative amplitudes at most wavelengths (Supporting Information Fig. S2_c). This spectral change would be expected if the tilt angle of the absorption dipole moment of retinal from the *c* axis (i.e., the membrane normal) is much smaller in N than in O. Interestingly, the N-to-O_1 transition (i.e., P_3 component) became undetectable at high concentrations of ammonium sulfate, where the decay of N appeared to be accelerated by the crystal lattice force. The O_1-to-O_2 transition was also undetected in the crystal, probably because the rate of this transition becomes relatively higher than the decay rate of M.

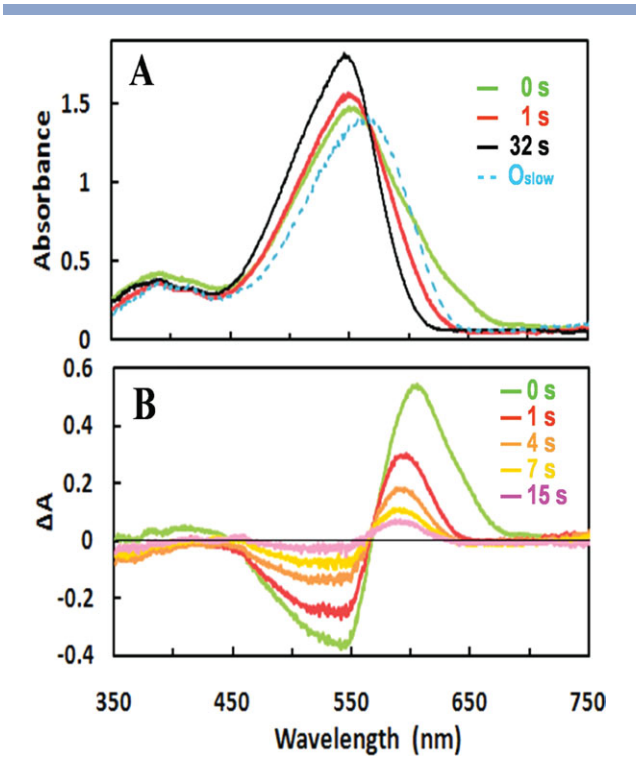

Figure 4

(**A**) Absorption spectra of the *P622* crystal of BR_L93A measured (i) after a crystal was flash-cooled under illumination with green light at 532 nm (~0.1 mW/mm^2) (green line), (ii) after the temperature of the illuminated crystal was transiently increased in the dark by blocking the stream of cold nitrogen gas for 1 s (red line), and (iii) in the dark-adapted state that was obtained after the crystal annealing (warming for 3–5 s + rapid cooling to 100K) was repeated several times. The broken blue line represents the most likely absorption spectrum of O_{slow}. In this experiment, a single crystal of BR_L93A was picked up with a nylon loop, soaked in a solution containing 3*M* ammonium sulfate, 0.1*M* Hepes buffer (pH 7.0) and 30% trehalose, and mounted at the sample stage in such a manner that the *c* axis was parallel to the measuring beam. (**B**) Difference absorption spectra associated with the thermal relaxations of O_{slow} and other reaction states. These spectra were derived by subtracting the absorption spectrum of the dark-adapted crystal from those recorded after various repetitions of the crystal annealing. The numerals indicate the accumulated time of the crystal warming (i.e., blockage of the cold nitrogen gas).

Trapping protocol for O_{slow} in crystals

To establish a suitable procedure for trapping O_{slow}, we investigated the spectroscopic properties of the *P622* crystal of BR_L93A under various illumination conditions. In Figure 4(A), the green line shows the absorption spectrum measured after a crystal soaked in 3.0*M* ammonium sulfate at pH 7.0 was flash-cooled to 100K under

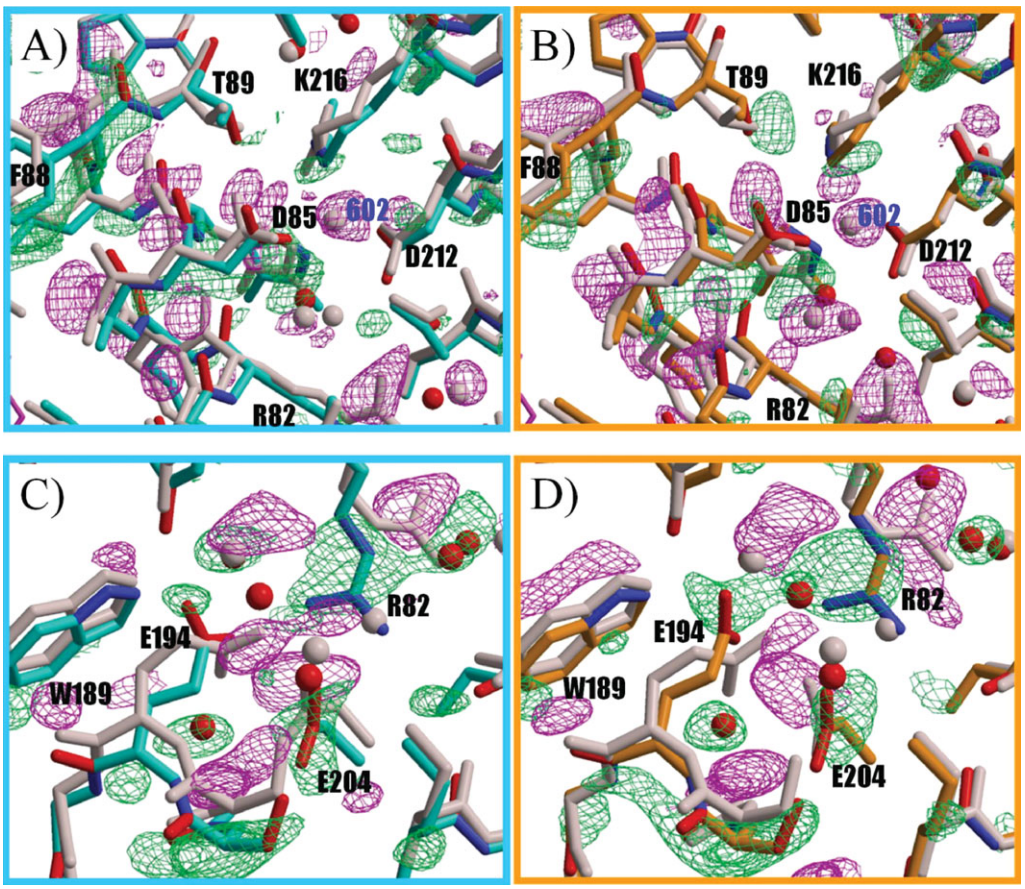

Figure 5

Light-induced structural changes in helix C (**A**, **B**) and in the proton release group (**C**, **D**) upon formation of O_{slow} of BR_L93A (left panels) and upon formation of M_{native} of native BR (right panels). The difference maps (positive densities in green, negative in purple) are contoured at 3.0 σ (A, C), 3.5 σ (B, D), respectively, and overlaid on the structural models of O_{slow} and the *trans* isomer of BR_L93A (left panels), and M_{native} and the *trans* isomer of native BR (right panels). Carbon atoms in O_{slow} and M_{native} are drawn in cyan and gold, respectively; oxygen atoms and water molecules in these states are shown in red; all the atoms in the *trans* isomers are shown in gray.

illumination with green light (at 532 nm). To remove the short-lived intermediates (such as K and M), the crystal was warmed again in the dark by blocking the stream of cold nitrogen gas for ∼1 s (Fig. 4). In this way, a considerable fraction of protein was trapped in O_{slow}. It will be shown later that ∼30% of the protein was trapped in O_{slow} when the crystal was flash-cooled with a delay of ∼1 s after the termination of green-light illumination. Thus it is likely that almost half of the protein was trapped under the illumination condition shown in Figure 4. In this case, the absorption spectrum of O_{slow} was calculated to have its absorption maximum (λ_{max}) at around 565 nm at 100K [the broken line in Fig. 4(A)]. Strictly speaking, the λ_{max} value is difficult to evaluate accurately. However, it can be argued safely that the peak absorbance of O_{slow} is much smaller (by ∼20%) than that of the *trans* isomer. This optical property of O_{slow} can be explained by supposing that the retinal chromophore takes on a 13-*cis* configuration in O_{slow}. This interpretation is supported by retinal extraction experiments, which showed that the content of 13-*cis* retinal increased significantly under light illumination (Supporting Information Table S2).

Structural changes induced upon formation of O_{slow}

The trapping procedure of O_{slow} mentioned above did not affect the crystal quality or the crystal lattice constants (Supporting Information Table S1). To evaluate a difference map between O_{slow} and the *trans* isomer, we compared the diffraction data (F_{green}) from a crystal that was flash-cooled after green-light illumination with those (F_{red}) from a crystal that was flash-cooled under illumination with red light at 650 nm (Supporting Information Fig. S3). Since O_{slow} was removed under red-light illumination, the following relationship was satisfied: $|F_{green}| - |F_{red}| = \alpha\ (|F_{O\text{-}slow}| - |F_{T\text{-}L93A}|)$, where α is the content

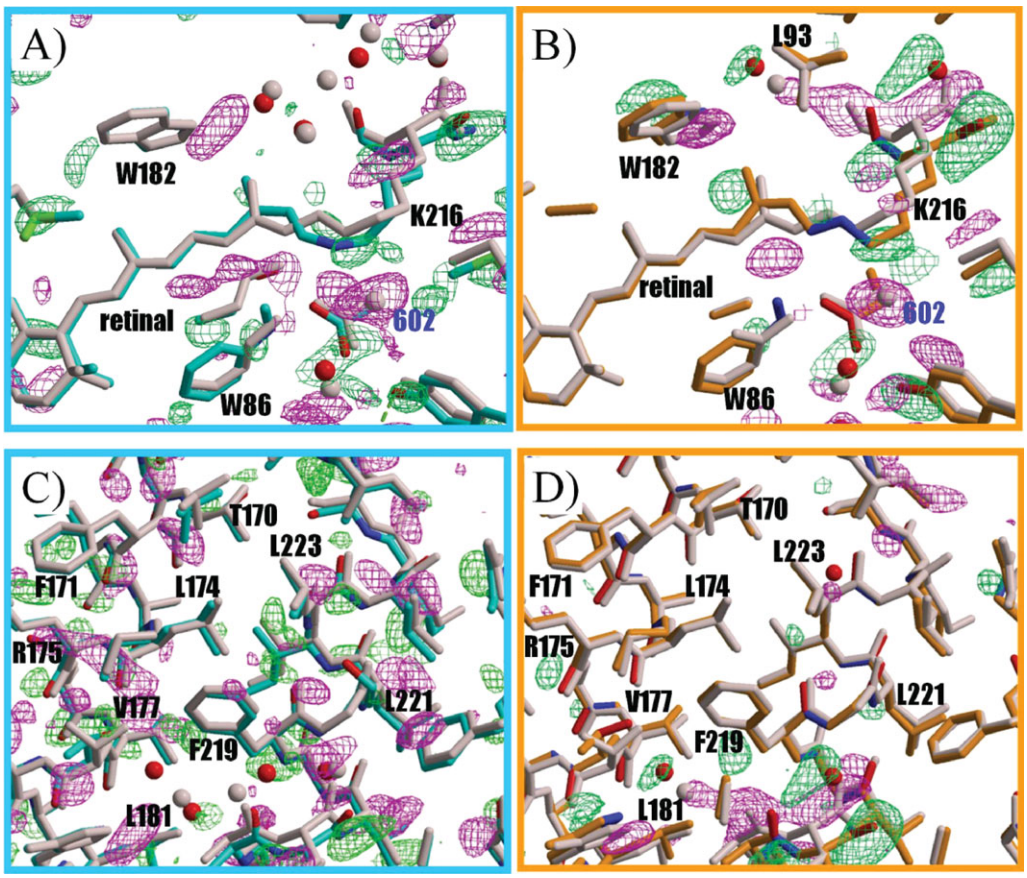

Figure 6

Light-induced structural changes in the retinal-Lys216 chain (**A**, **B**) and in helices F and G (**C**, **D**) upon formation of O_{slow} of BR_L93A (left panels) and upon formation of M_{native} of native BR (right panels). The difference maps (positive densities in green, negative in purple) are contoured at 2.6 σ (A, C), and 3.2σ (B, D), respectively, and overlaid on the structural models of O_{slow} and the *trans* isomer of BR_L93A (left panels), and M_{native} and the *trans* isomer of native BR (right panels). Carbon atoms in O_{slow} and M_{native} are drawn in cyan and gold, respectively; oxygen atoms and water molecules in these states are shown in red; all the atoms in the *trans* isomers are shown in gray.

of O_{slow} in the crystal that was flash-cooled after green-light illumination.

In the $|F_{green}| - |F_{red}|$ difference map, the most pronounced changes induced upon the formation of O_{slow} are confined to the extracellular half of helix C and the FG loop. Interestingly, this difference map is similar in profile to the previously reported $|F_{M\text{-}native}| - |F_{T\text{-}native}|$ difference map between M_{native} and the *trans* isomer (T_{native}) of native BR.[20] Although most positive/negative peaks in the $|F_{green}| - |F_{red}|$ map are less significant than in the $|F_{M\text{-}native}| - |F_{T\text{-}native}|$ map, this is because the trapping efficiency of O_{slow} is much lower than that of the M intermediate of native BR.

To make it easier to investigate how the structure of O_{slow} is correlated with that of M_{native}, the $|F_{green}| - |F_{red}|$ and $|F_{M\text{-}native}| - |F_{T\text{-}native}|$ difference maps are contoured at different levels in Figure 5. Similarity between the $|F_{green}| - |F_{red}|$ map and the $|F_{M\text{-}native}| - |F_{T\text{-}native}|$ map is clearly seen in enlarged views around the middle moiety of helix C and the proton release group (Fig. 5). The common features shared by these structural changes are summarized as follows: (1) disappearance of the water (Wat602) that interacts with the Schiff base in the unphotolyzed state; (2) deformation of the extracellular half of helix C (Arg82 through Phe88) and a profound swing in the side chain of Phe88; (3) a flip-flop movement of the side chain of Arg82 and disruption of the paired structure of Glu194 and Glu204; (4) sliding movement of the extracellular half of helix G toward the extracellular side, which is associated with a large deformation of the FG loop.

Close investigation of the $|F_{green}| - |F_{red}|$ and $|F_{M\text{-}native}| - |F_{T\text{-}native}|$ maps shows that there are two major differences between M_{native} and O_{slow}. First, the negative/positive peaks around the retinal-Lys216 chain are less significant in the $|F_{green}| - |F_{red}|$ map than in the $|F_{M\text{-}native}| - |F_{T\text{-}native}|$ map (Fig. 6). Second, the $|F_{green}| - |F_{red}|$ map exhibits small positive/negative peaks along

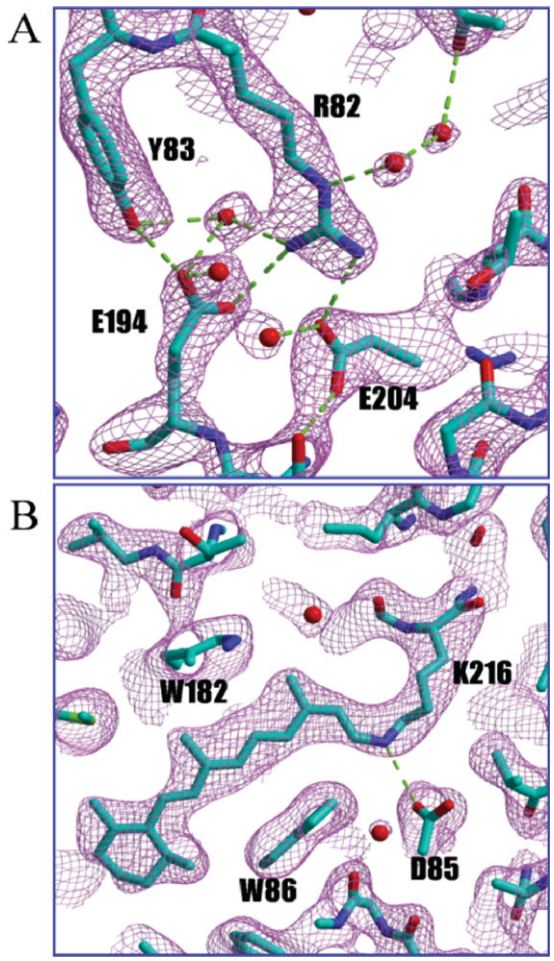

Figure 7

$2F_o$–F_c maps in the proton-release channel (**A**) and the retinal-binding site (**B**) of O_{slow} at pH 7.0, contoured at 1.0 σ and 1.2 σ, respectively, and overlaid on the structural model. Carbon, nitrogen, and oxygen atoms are drawn in cyan, blue, and red, respectively. [Color figure can be viewed in the online issue, which is available at wileyonlinelibrary.com.]

helix F, whereas these peaks are not clearly seen in the $|F_{M\text{-native}}| - |F_{T\text{-native}}|$ map (Fig. 6).

Structure of O_{slow}

Figure 7 shows the structural model of O_{slow}, which was built on the assumption that O_{slow} was completely removed under red-light illumination, while one third of the protein was trapped in O_{slow} when the crystal was flash-cooled 0.5 s after the green light was turned off. During the model building, the content of O_{slow}, α, was adjusted until the $2F_o$-F_c map of O_{slow} showed clear densities around the water molecules in the vicinity of Arg82 [Fig. 7(A)]. The optimal value of α obtained by this procedure is similar to that estimated by another procedure of refinement in which the observed structural factor $|F_{green}|$ was compared with a weighted average of the calculated structural factors of the two conformers (O_{slow} and the *trans* isomer) (Supporting Information Fig. S4).

Examination of all possible configurations of the retinal-Lys216 chain revealed that the 13-*cis*/15-*syn* configuration was most compatible with the omit map of retinal [Fig. 7(B)]. In this case, retinal takes on a planar configuration so that the Schiff base is orientated toward the extracellular side and interacts with Asp85. Trials of model building with the 13-*cis*/15-*anti* configuration resulted in worse fitting even when unusually large twisting around the C13=C14 bond or the Schiff base linkage was introduced (Supporting Information Fig. S5). Since no mechanism stabilizing a largely twisted retinal has been found, we prefer the structural model of O_{slow} in which retinal takes on the planar 13-*cis*/15-*syn* configuration. [We gave up adopting a model with 13-*cis*/15-*anti* retinal, in which the distance between the Schiff base and the closest water molecule (Wat701) was 3.7 Å (too far to make a hydrogen bond), while Wat701 was not hydrogen-bonded to any other group.] Meanwhile, a model with all-*trans* retinal, by which the omit map may be fitted, is not compatible with the result of retinal extraction experiments (Supporting Information Table S2).

The configuration of retinal in O_{slow} is similar to that found in the 13-*cis* isomer contained in the dark-adapted state of native BR.[44] However, there is a large difference between O_{slow} and the 13-*cis* isomer of native BR (13-*cis*-BR) in terms of the structure of the protein moiety. For example, (1) 13-*cis*-BR has a water molecule (Wat602) in a cavity between Asp85 and the Schiff base, while this water is squeezed out from the active site in O_{slow}; (2) the structure of helix C is largely deformed in O_{slow}, whereas it is barely altered in 13-*cis*-BR.

As expected from the difference maps, the protein structure of O_{slow} is rather similar to that of M_{native} (Supporting Information Fig. S5). In both these states, the paired structure of Glu194 and Glu204 is broken, and the side chain of Arg82 points toward the extracellular side to make salt bridges with Glu194 and Glu204 (Supporting Information Fig. S6). The major differences between O_{slow} and M_{native} are as follows: (1) the main-chain conformation of Lys216 is less distorted in O_{slow} than in M_{native}; (2) a noticeable sliding of the cytoplasmic half of helix G toward the extracellular side and the deformation of helix F around Arg175 are induced upon the formation of O_{slow}, while these movements are not evident upon the formation of M_{native}. The possibility that the deformation of helix F is attributable to the presence of a small amount of N in O_{slow} will be discussed later.

pH dependence of the conformation of the proton release group

The *P622* crystal of BR_L93A is stable in a wide pH range, making it possible to investigate the dependence

of the protein structures in both the *trans* isomer and O_{slow} on pH. The structure of the *trans* isomer was found to be unaltered when the pH of the postcrystallization solution was increased from pH 4.5 to pH 9.3. When the pH of the medium was decreased to pH 3.0, however, BR_L93A underwent an acid transition that was accompanied by a large red shift of the visible band (λ_{max}: 540 nm → 560 nm). Diffraction data from a crystal soaked at pH 3.0 showed that this acidification caused a significant shrinkage of the *P622* crystal along the *c* axis (Supporting Information Table S1). This shrinkage was accompanied by disorder of the BC loop, as observed upon the acid transition of native BR.[24] The structural analysis showed that the acid transition of BR_L93A is accompanied by disruption of the paired structure of Glu194 and Glu204 and the flip-flop movement of the side chain of Arg82 toward the extracellular side. This structural change is essentially the same as that observed for the acid blue transition of native BR. As long as the structure of the proton release channel is discussed, the structural changes induced upon the acid blue transition do not differ much from those induced upon the formations of M_{native} and O_{slow}.

It has previously been shown that the paired structure of Glu194 and Glu204 in the proton-release group is completely destroyed when the M state is generated at pH 7.0 or higher, whereas this destruction is incomplete when the M state is generated at an acidic pH.[20] To investigate how the structure of the proton release group (i.e., Glue194/Glu204) in O_{slow} is dependent on the pH of the medium, we collected diffraction data from a crystal that was soaked at pH 4.5 and then flash-cooled after green-light illumination. We found that the paired structure of Glu194 and Glu204 was completely destroyed even when O_{slow} was generated at pH 4.5. This result suggests that the pK_a value of the proton release group is much lower in O_{slow} than in M_{native}. A similar relationship was previously observed for M and O in suspension of native BR.[45]

DISCUSSION

Formation pathway of O_{slow}

The most remarkable effect of the Leu93→Ala replacement is the appearance of a long-lived substate of the O intermediate, which is referred as O_{slow}. However, the formation pathway of O_{slow} has remained unsolved. It has been reported that the dark adaptation of native BR occurs very rapidly in the acid blue form.[46] Since the structure of O_{slow} does not differ much from that of the acid blue form, we can suppose that retinal isomerization from the all-*trans* to 13-*cis*/15-*syn* configuration occurs during the extended lifetime of O. This supposition is congruent with the difference absorption spectrum associated with the P_4 component, whose profile resembles the spectral change associated with the dark adaptation of native BR (i.e., the interconversion from the *trans* isomer to the 13-*cis* isomer) (Fig. 2).

The spectral and structural data suggest that the extended lifetime of O in BR_L93A is an indirect effect of the side reaction (N→ O_1 (↔ O_2) → *trans*-BR) or the branching reaction (N→ O_1 → O_2 → 13-*cis*-BR→ *trans*-BR) [Fig. 3(A)]. [In the latter case, the transition from 13-*cis*-BR to *trans*-BR was suggested to be very rapid because no spectral change was observed upon light/dark adaptation of BR_L93A.[24]] In both cases, the recovery of the initial state would be expected to accelerate when the O_1 → O_2 transition is blocked. Previously, Delaney *et al.* have observed that the photocycle of BR_L93A becomes normal when the rotational freedom around the C10-C11 or C12-C13 single bond is reduced.[47] This curious but important phenomenon is understandable by supposing that the O_1 → O_2 transition is inhibited by reducing the flexibility of the polyene chain of retinal. On the other hand, red light is effective at removing O_{slow}. Together with a previous report that the proton pumping rate of BR_L93A under illumination with strong light is close to that of native BR,[27] the present observation suggests that the light-initiated inter-conversion from the 13-*cis*/15-*syn* configuration (O_2) to the *trans* isomer (*trans*-BR) takes place much more efficiently than the light adaptation of native BR [Fig. 3(A)]. Otherwise, we have to suppose that a non-negligible amount of N with 13-*cis*/15-*anti* retinal co-exists in O_{slow}.

It has generally been believed that the formation efficiency of O_2 (i.e., the substate of O with the 13-*cis*/15-*syn* retinal) is not high in the *trans* photocycle of native BR, in which O_1 (i.e., the substate with the all-*trans* retinal) relaxes rapidly into the initial state.[5] It has been reported, however, that the branching reaction from the *trans* photocycle to the 13-*cis* isomer becomes significant under some experimental conditions (e.g., in a dried film of purple membrane[48] and in a solubilized state[49]). These phenomena can be explained well by supposing that O_2 is generated efficiently and a large fraction of O_2 relaxes into the 13-*cis* isomer. It has been known that the transient concentration of O after the excitation of native BR increases with temperature.[50] For better understanding of the last steps of the proton pumping cycle of BR_L93A, it is important to further refine the reaction scheme in which O_2 is included [Fig. 3(A)]. It should be noticed that the O_1 → O_2 transition in BR_L93A is much slower than the decay of O in native BR. This observation suggests that the steric interaction between the side chain of Leu93 and the 13-methyl of retinal plays an important role in accelerating the recovery of the initial protein conformation (*trans*-BR).

Role of internal water molecules on the color tuning

The structural model of the *trans* isomer of BR_L93A shows that the deletion of three carbon atoms in Leu93 is compensated for by the insertion of four water molecules in the cytoplasmic vicinity of retinal. Since the

structure of the retinal-binding pocket is barely affected by the mutation, the inserted water molecules may be responsible for the large blue shift of the visible band (λ_{max}: 570 nm → 540 nm). It is noteworthy that the water molecule (Wat701) in the vicinity of the C13 methyl of retinal interacts weakly with the surrounding residues. Owing to its motional freedom, this water can contribute to a substantial increase in the local dielectric constant. In such an environment, the ground state of retinal with a protonated Schiff base would be relatively more stable than its excited state, leading to a large blue shift of the visible band.

The visible band of O_{slow} ($\lambda_{max} \sim 565$ nm) is red-shifted compared with that of the initial state ($\lambda_{max} \sim 540$ nm). A similar red shift is induced upon formation of the acid blue form of BR_L93A. Since the structure of the proton release channel of O_{slow} does not differ much from that of the acid blue form, the red-shifted λ_{max} of O_{slow} is attributable to the protonation of Asp85 (or Asp212). Roughly speaking, the magnitude of the red shift induced by the purple-to-blue transition is conserved between BR_L93A and native BR; that is, the λ_{max} value at room temperature shifts from 540 nm to 560 nm upon acidification of BR_L93A, while it shifts from 570 nm to 600 nm upon acidification of native BR.[51] It can be argued that the color tuning of BR is controlled independently by the distribution of water in the cytoplasmic vicinity of the Schiff base and the charge distribution in the extracellular vicinity of the Schiff base.

A remarkable effect of the insertion of water in the cytoplasmic vicinity of retinal is the stabilization of the L intermediate at neutral pH; that is, the equilibrium between L and M is shifted toward L in BR_L93A (Fig. 2). One may argue that the stabilization of a conformer containing the 13-*cis*/15-*anti* retinal with the protonated Schiff base is attributable to the absence of steric conflict between the C13 methyl and the side chain of Leu93. However, a more likely explanation is that the pK_a value of the Schiff base in an equilibrium state between L and M is kept high owing to the formation of a stable hydrogen bond between the protonated Schiff base and one of the water molecules inserted in the large cavity around Ala93. Although the same hydrogen bond is formed in the L intermediate of native BR, this is only accomplished by distortion of the surrounding structure, including rotation of the side chain of Leu93.[12] In the M intermediate of native BR, the side chain of Leu93 is reorientated to block the approach of water to the Schiff base.[19] As a result of this blocking, the pK_a value of the Schiff base is very low (p$K_a < 4.5$) in M_{native}.[20]

Deformation of helix C during the photocycles of archaeal rhodopsins

Despite their different spectral properties, the structures of O_{slow} and M_{native} are similar to each other. In fact, the structure of the proton release channel is identical in O_{slow} and M_{native}. This similarity implies that the proton release channel can take on a limited number of conformations during the proton pumping cycle. Recent structural analyses of pharaonis halorhodopsin (*p*HR), a light-driven anion pump, have shown that the extracellular half of helix C is deformed upon the formation of an O-like blue form or an anion-depleted yellow form.[52] The deformation of helix C allows one chloride ion and one water molecule to be expelled from a cavity in the extracellular vicinity of the Schiff base. Since most key residues (Arg82, Tyr83, Trp86, Thr90, and Pro91) in helix C are conserved between BR and pHR,[53] it is not surprising that the deformation of helix C during the ion pumping cycle takes place in a similar fashion in BR and *p*HR. The strong correlation between the light-induced structural changes of these archaeal rhodopsins is understandable in the context of a recent hypothesis that BR functions as a proton/water antiporter, while HR functions as a proton/HCl antiporter.[54] It is possible that the extracellular half of helix C functions as a sort of valve by which the unidirectional movement of ions is achieved.

Conceptually, it has been postulated that the proton uptake pathway undergoes a large structural change in the M-to-N transition.[7,55] Previous structural analyses of the N intermediate of native BR have shown that the cytoplasmic half of helix F tilts outward upon the formation of N.[21] The large structural change of the EF loop in the M-to-N transition has been suggested by many experimental data, including the previous observation that the decay of M is inhibited by the crystal lattice force.[20] It is shown here that the N intermediate is destabilized by the crystal lattice force (Supporting Information Fig. S2). It is likely that the EF loop is greatly distorted in this reaction state. Conversely, the structure of the EF loop in O_{slow} does not differ much from that in M_{native}. It is thus suggested that the large conformational change in the EF loop that takes place in the M-to-N transition is reverted before the formation of O_{slow}.

It should be mentioned, however, that there are noticeable differences between O_{slow} and M_{native} in terms of protein structure (Figs. 5 and 6). The observation that the main chain conformation of Lys216 is less distorted in O_{slow} than in M_{native} is readily explained by taking into account the fact that the retinal in O_{slow} takes on the 13-*cis*/15-*syn* configuration, while it takes on the 13-*cis*/15-*anti* configuration in M_{native}. Particularly noteworthy is the observation that the cytoplasmic moiety of helix F is deformed in O_{slow}; that is, several residues around Arg175 move outwards upon the formation of O_{slow}, while these movements are not seen in M_{native}. It appears that the deformation of helix F in O_{slow} represents an afterimage of a larger structural change occurring at an earlier stage. An alternative explanation is that a small amount of N is present in O_{slow}. It has been suggested

from the structural analysis of purple membrane by electron microscopy that the cytoplasmic half of helix F deforms largely in the N intermediate.[21] Although the N intermediate was suggested to be destabilized in the *P622* crystal,[20] the possibility that a small amount of N coexists in O_{slow} cannot be excluded. In this case, the structure of O_{slow} should be regarded as a weighted average of the structures of N and O_2. To discuss this possibility, we need to carry our more comprehensive studies including the structural analysis of the pure state of N, which may be achieved by preparing such a three-dimensional crystal that a large conformational change of helix F is allowed.

ACKNOWLEDGMENTS

Coordinates and structural parameters for the *trans* isomer and the O intermediate of BR_L93A have been deposited with the Protein Data Bank under accession codes: 3VHZ and 3VI0.

REFERENCES

1. Henderson R, Baldwin JM, Ceska TA, Zemlin F, Beckmann E, Downing KH. Model for the structure of bacteriorhodopsin based on high-resolution electron cryo-microscopy. J Mol Biol 1990;213: 899–929.
2. Phatak P, Ghosh N, Yu H, Cui Q, Elstner M. Amino acids with an intermolecular proton bond as proton storage site in bacteriorhodopsin. Proc Natl Acad Sci USA 2008;105:19672–19677.
3. Watanabe HC, Ishikura T, Yamato T. Theoretical modeling of the O-intermediate structure of bacteriorhodopsin. Proteins 2009;75: 53–61.
4. Bondar AN, Fischer S, Smith JC. Water pathways in the bacteriorhodopsin proton pump. J Membr Biol 2011;239:73–84.
5. Ames JB, Mathies RA. The role of back-reactions and proton uptake during the N----O transition in bacteriorhodopsin's photocycle: a kinetic resonance Raman study. Biochemistry 1990;29:7181–7190.
6. Der A, Keszthelyi L. Charge motion during the photocycle of bacteriorhodopsin. Biochemistry (Mosc) 2001;66:1234–1248.
7. Lanyi JK. Studies of the bacteriorhodopsin photocycle without the use of light: clues to proton transfer coupled reactions. J Mol Microbiol Biotechnol 2007;12:210–217.
8. Edman K, Nollert P, Royant A, Belrhali H, Pebay-Peyroula E, Hajdu J, Neutze R, Landau EM. High-resolution X-ray structure of an early intermediate in the bacteriorhodopsin photocycle. Nature 1999;401:822–826.
9. Schobert B, Cupp-Vickery J, Hornak V, Smith S, Lanyi J. Crystallographic structure of the K intermediate of bacteriorhodopsin: conservation of free energy after photoisomerization of the retinal. J Mol Biol 2002;321:715–726.
10. Matsui Y, Sakai K, Murakami M, Shiro Y, Adachi S, Okumura H, Kouyama T. Specific damage induced by X-ray radiation and structural changes in the primary photoreaction of bacteriorhodopsin. J Mol Biol 2002;324:469–481.
11. Royant A, Edman K, Ursby T, Pebay-Peyroula E, Landau EM, Neutze R. Helix deformation is coupled to vectorial proton transport in the photocycle of bacteriorhodopsin. Nature 2000;406:645–648.
12. Kouyama T, Nishikawa T, Tokuhisa T, Okumura H. Crystal structure of the L intermediate of bacteriorhodopsin: evidence for vertical translocation of a water molecule during the proton pumping cycle. J Mol Biol 2004;335:531–546.
13. Lanyi JK, Schobert B. Structural changes in the L photointermediate of bacteriorhodopsin. J Mol Biol 2007;365:1379–1392.
14. Luecke H, Schobert B, Richter HT, Cartailler JP, Lanyi JK. Structural changes in bacteriorhodopsin during ion transport at 2 angstrom resolution. Science 1999;286:255–261.
15. Sass HJ, Buldt G, Gessenich R, Hehn D, Neff D, Schlesinger R, Berendzen J, Ormos P. Structural alterations for proton translocation in the M state of wild-type bacteriorhodopsin. Nature 2000; 406:649–653.
16. Facciotti MT, Rouhani S, Burkard FT, Betancourt FM, Downing KH, Rose RB, McDermott G, Glaeser RM. Structure of an early intermediate in the M-state phase of the bacteriorhodopsin photocycle. Biophys J 2001;81:3442–3455.
17. Luecke H, Schobert B, Cartailler JP, Richter HT, Rosengarth A, Needleman R, Lanyi JK. Coupling photoisomerization of retinal to directional transport in bacteriorhodopsin. J Mol Biol 2000;300: 1237–1255.
18. Lanyi JK, Schobert B. Mechanism of proton transport in bacteriorhodopsin from crystallographic structures of the K, L, M_1, M_2, and $M_{2'}$ intermediates of the photocycle. J Mol Biol 2003;328:439–450.
19. Takeda K, Matsui Y, Kamiya N, Adachi S, Okumura H, Kouyama T. Crystal structure of the M intermediate of bacteriorhodopsin: allosteric structural changes mediated by sliding movement of a transmembrane helix. J Mol Biol 2004;341:1023–1037.
20. Yamamoto M, Hayakawa N, Murakami M, Kouyama T. Crystal structures of different substrates of bacteriorhodopsin's M intermediate at various pH levels. J Mol Biol 2009;393:559–573.
21. Vonck J. Structure of the bacteriorhodopsin mutant F219L N intermediate revealed by electron crystallography. EMBO J 2000;19: 2152–2160.
22. Schobert B, Brown LS, Lanyi JK. Crystallographic structures of the M and N intermediates of bacteriorhodopsin: Assembly of a hydrogen-bonded chain of water molecules between Asp-96 and the retinal Schiff BASE. J Mol Biol 2003;330:553–570.
23. Rouhani S, Cartailler JP, Facciotti MT, Walian P, Needleman R, Lanyi JK, Glaeser RM, Luecke H. Crystal structure of the D85S mutant of bacteriorhodopsin: model of an O-like photocycle intermediate. J Mol Biol 2001;313:615–628.
24. Okumura H, Murakami M, Kouyama T. Crystal structures of acid blue and alkaline purple forms of bacteriorhodopsin. J Mol Biol 2005;351:481–495.
25. Subramaniam S, Greenhalgh DA, Rath P, Rothschild KJ, Khorana HG. Replacement of leucine-93 by alanine or threonine slows down the decay of the N and O intermediates in the photocycle of bacteriorhodopsin: implications for proton uptake and 13-cis-retinal----all-trans-retinal reisomerization. Proc Natl Acad Sci USA 1991;88: 6873–6877.
26. Subramaniam S, Faruqi AR, Oesterhelt D, Henderson R. Electron diffraction studies of light-induced conformational changes in the Leu-93-->Ala bacteriorhodopsin mutant. Proc Natl Acad Sci USA 1997;94:1767–1772.
27. Subramaniam S, Lindahl M, Bullough P, Faruqi AR, Tittor J, Oesterhelt D, Brown L, Lanyi J, Henderson R. Protein conformational changes in the bacteriorhodopsin photocycle. J Mol Biol 1999;287: 145–161.
28. Toth-Boconadi R, Keszthelyi L, Stoeckenius W. Late events in the photocycle of bacteriorhodopsin mutant L93A. Biophys J 2003;84: 3848–3856.
29. Cline SW, Schalkwyk LC, Doolittle WF. Transformation of the archaebacterium *Halobacterium volcanii* with genomic DNA. J Bacteriol 1989;171:4987–4991.
30. Boeke JD, LaCroute F, Fink GR. A positive selection for mutants lacking orotidine-5′-phosphate decarboxylase activity in yeast: 5-fluoro-orotic acid resistance. Mol Gen Genet 1984;197:345–346.
31. Oesterhelt D, Stoeckenius W. Rhodopsin-like protein from the purple membrane of *Halobacterium halobium*. Nat New Biol 1971;233:149–152.

32. Takeda K, Sato H, Hino T, Kono M, Fukuda K, Sakurai I, Okada T, Kouyama T. A novel three-dimensional crystal of bacteriorhodopsin obtained by successive fusion of the vesicular assemblies. J Mol Biol 1998;283:463–474.
33. Sakai K, Matsui Y, Kouyama T, Shiro Y, Adachi S-I. Optical monitoring of freeze-trapped reaction intermediates in protein crystals: a microspectrophotometer for cryogenic protein crystallography. J Appl Crystallogr 2002;35:270–273.
34. Kouyama T, Nasuda-Kouyama A, Ikegami A, Mathew MK, Stoeckenius W. Bacteriorhodopsin photoreaction: identification of a long-lived intermediate N (P,R350) at high pH and its M-like photoproduct. Biochemistry 1988;27:5855–5863.
35. Hayakawa N, Kasahara T, Hasegawa D, Yoshimura K, Murakami M, Kouyama T. Effect of xenon binding to a hydrophobic cavity on the proton pumping cycle in bacteriorhodopsin. J Mol Biol 2008;384: 812–823.
36. Chizhov I, Chernavskii DS, Engelhard M, Mueller KH, Zubov BV, Hess B. Spectrally silent transitions in the bacteriorhodopsin photocycle. Biophys J 1996;71:2329–2345.
37. Chan TF. An improved algorithm for computing the singular value decomposition. ACM Trans Math Softw 1982;8:72–83.
38. Steller I, Bolotovsky R, Rossmann MG. An algorithm for automatic indexing of oscillation images using Fourier analysis. J Appl Crystallogr 1997;30:1036–1040.
39. Dodson EJ, Winn M, Ralph A. Collaborative computational project, number 4: providing programs for protein crystallography. Methods Enzymol 1997;277:620–633.
40. Brunger AT, Adams PD, Clore GM, DeLano WL, Gros P, Grosse-Kunstleve RW, Jiang JS, Kuszewski J, Nilges M, Pannu NS, Read RJ, Rice LM, Simonson T, Warren GL. Crystallography & NMR system: a new software suite for macromolecular structure determination. Acta Crystallogr D Biol Crystallogr 1998;54:905–921.
41. McRee DE. Practical Protein Crystallography. San Diego: Academic Press; 1993.
42. Maeda A, Tomson FL, Gennis RB, Balashov SP, Ebrey TG. Water molecule rearrangements around Leu93 and Trp182 in the formation of the L intermediate in bacteriorhodopsin's photocycle. Biochemistry 2003;42:2535–2541.
43. Balashov SP, Imasheva ES, Govindjee R, Ebrey TG. Titration of aspartate-85 in bacteriorhodopsin: what it says about chromophore isomerization and proton release. Biophys J 1996;70:473–481
44. Nishikawa T, Murakami M, Kouyama T. Crystal structure of the 13-cis isomer of bacteriorhodopsin in the dark-adapted state. J Mol Biol 2005;352:319–328.
45. Balashov SP, Lu M, Imasheva ES, Govindjee R, Ebrey TG, Othersen B, III, Chen Y, Crouch RK, Menick DR. The proton release group of bacteriorhodopsin controls the rate of the final step of its photocycle at low pH. Biochemistry 1999;38:2026–2039.
46. Balashov SP, Imasheva ES, Govindjee R, Ebrey TG. Titration of aspartate-85 in bacteriorhodopsin: what it says about chromophore isomerization and proton release. Biophys J 1996;70:473–481.
47. Delaney JK, Yahalom G, Sheves M, Subramaniam S. Reducing the flexibility of retinal restores a wild-type-like photocycle in bacteriorhodopsin mutants defective in protein-retinal coupling. Proc Natl Acad Sci USA 1997;94:5028–5033.
48. Kouyama T, Bogomolni RA, Stoeckenius W. Photoconversion from the light-adapted to the dark-adapted state of bacteriorhodopsin. Biophys J 1985;48:201–208.
49. Casadio R, Gutowitz H, Mowery P, Taylor M, Stoeckenius W. Light-dark adaptation of bacteriorhodopsin in triton-treated purple membrane. Biochim Biophys Acta 1980;590:13–23.
50. Chizhov I, Engelhard M, Chernavskii DS, Zubov B, Hess B. Temperature and pH sensitivity of the O(640) intermediate of the bacteriorhodopsin photocycle. Biophys J 1992;61:1001–1006.
51. Mowery PC, Lozier RH, Chae Q, Tseng YW, Taylor M, Stoeckenius W. Effect of acid pH on the absorption spectra and photoreactions of bacteriorhodopsin. Biochemistry 1979;18:4100–4107.
52. Kanada S, Takeguchi Y, Murakami M, Ihara K, Kouyama T. Crystal structures of an O-like blue form and an anion-free yellow form of pharaonis halorhodopsin. J Mol Biol 2011;413:162–176.
53. Ihara K, Umemura T, Katagiri I, Kitajima-Ihara T, Sugiyama Y, Kimura Y, Mukohata Y. Evolution of the archaeal rhodopsins: evolution rate changes by gene duplication and functional differentiation. J Mol Biol 1999;285:163–174.
54. Kouyama T, Kanada S, Takeguchi Y, Narusawa A, Murakami M, Ihara K. Crystal structure of the light-driven chloride pump halorhodopsin from *Natronomonas pharaonis*. J Mol Biol 2010;396:564–579.
55. Oka T, Yagi N, Fujisawa T, Kamikubo H, Tokunaga F, Kataoka M. Time-resolved x-ray diffraction reveals multiple conformations in the M-N transition of the bacteriorhodopsin photocycle. Proc Natl Acad Sci USA 2000;97:14278–14282.